CLM - P 417

This document is intended for publication in a journal, and is made available on the understanding that extracts or references will not be published prior to publication of the original, without the consent of the author.

CLM - P 417

CULHAM LABORATORY
LIBRARY
13 AUG 1975
6

UKAEA RESEARCH GROUP

Preprint

LABORATORY INVESTIGATION OF SHOCK WAVES IN A WEAKLY MAGNETISED PLASMA

A D CRAIG

CULHAM LABORATORY
Abingdon Oxfordshire

1975

This document is intended for publication in a journal or at a conference and is made available on the understanding that extracts or references will not be published prior to publication of the original, without the consent of the authors.

Enquiries about copyright and reproduction should be addressed to the Librarian, UKAEA, Culham Laboratory, Abingdon, Oxfordshire, England

CLM-P 417

LABORATORY INVESTIGATION OF SHOCK WAVES IN A WEAKLY MAGNETISED PLASMA

A.D. Craig

Euratom, UKAEA Association for Fusion Research,
Culham Laboratory, Abingdon, Oxon, OX14 3DB, UK

ABSTRACT

Experimental measurements of the structure of collision dominated shock waves propagating into a weakly magnetised hydrogen plasma are described. The initial magnetic field is varied in the range 0.035 T to zero with corresponding Alfven Mach number in the range 2.5 to infinity and sonic Mach number in the range 6.5 to 2. At the lower field values the influence of the magnetic field on the shock dissipation is negligible. The measured shock structure is in general agreement with theoretical non-magnetic shock structure based on a two fluid model with classical transport coefficients in that (i) a precursor thermal wave exists ahead of the velocity transition, (ii) the velocity transition occurs in a distance $\sim 2\lambda_{ii2}$ where λ_{ii2} is the ion mean free path in the post-shock region, (iii) the electron heating within the shock is comparable with the ion heating.

(Submitted for publication in Plasma Physics)

February 1975
KS

1. INTRODUCTION

This paper describes experimental measurements of the structure of collision dominated shock waves propagating in a weakly magnetised hydrogen plasma. The initial magnetic field is varied in the range 0.035 T to zero with corresponding Alfven Mach number (M_A) in the range 2.5 to infinity and sonic Mach (M_s) in the range 6.5 to 2. Propagation is at approximately 30^o to the initial magnetic field throughout this range. At the lower field values ($\lesssim$ 0.01 T) the plasma β ($= 2 \mu nk (T_e + T_i)/B^2$) $>> 1$ and gyration effects are not important ($\omega_{ce} \tau_{ee} < 1$). We therefore compare the experimental shock structure with theoretical non-magnetic shock structure. However the magnetic Reynolds number in these shocks is large ($\sim 10^2$) and hence the transverse magnetic field is compressed within the shock. This provides a useful means of identifying the shock and hence measuring its dynamics.

A previous paper (CRAIG, 1974) has described measurements on oblique and parallel hydromagnetic shocks in a lower M_A regime with initial magnetic fields in the range 0.1 to 0.2 T. Good reproducibility and a clear separation of the shock from its driving piston in this previous work has stimulated the extension of the work to the higher M_A regime discussed in the present paper.

Several theoretical approaches to the problem of plane collisional non-magnetic shock structure have been made. JUKES (1957-58) assumes that two species of particles, electrons and protons, behave separately, each being in a quasi-equilibrium state corresponding to separate temperatures, T_e and T_i. Navier-Stokes type of equations with classical coefficients of viscosity and thermal conductivity appropriate to the two species are solved by numerical iteration. He finds that for strong shock waves (sonic Mach number $M_s \gtrsim 2$),

(a) Number density n and ion temperature T_i change in $\sim 2\lambda_{ii2}$ where λ_{ii2} is the ion-ion mean free path in the post-shock region.

(b) Electron thermal conduction leads to a precursor thermal wave extending a distance $\sim 5\lambda_{ii2}$ ahead of the density rise.

(c) Post-shock ion temperature T_{i2} is only slightly higher than the post-shock electron temperature T_{e2}.

Several experimental investigations (TAYLOR et al., 1970; COHN and MACKENZIE, 1972; HONZANA, 1973) have been made of collisionless electrostatic shocks where dispersive structures with a thickness considerably smaller than the ion-ion collision length have been observed. However very little experimental work has been done on collisional non-magnetic shocks in almost fully ionised plasma. The only instance known to the author is by BOGEN et al (1971) who produce shocks in a pre-heated theta pinch plasma containing only a weak transverse magnetic field (< 0.013 T). Using the Thomson scattering technique they observe the theoretically predicted precursor electron thermal wave.

2. APPARATUS (Fig. 1)

The discharge chamber, consisting of a Pyrex glass cylinder 1.2 m long and 0.46 m in diameter, is immersed in a uniform axial magnetic field $B_{z1} < 0.035$ T. An initial hydrogen plasma (filling pressure = 40 mtorr) is formed by a high current discharge between electrodes A and B. After 350 μsec from the initiation of the discharge a quiescent initial plasma exists with electron density $n_{e1} \sim 3 \times 10^{20}$ m^{-3} and temperature $T_{e1} \sim 1.2$ eV (as measured using a Langmuir probe previously calibrated against a He-Ne laser interferometer (CRAIG and PAUL, 1973)) in the region $80 \lesssim r \lesssim 180$ mm. No direct measurement of the neutral atom density n_n was made. However

we draw on the similarity between the present experiment and the Tarantula experiment, for which measurements (PAUL, 1970) show $n_n \approx 0.1\, n_e$ in a hydrogen plasma at the same temperature ($T_e \sim 1.2$ eV) and comparable density ($n_e \sim 6 \times 10^{20}$ m^{-3}). In the following sections we therefore consider the plasma to be fully ionised.

The main radial discharge is produced by applying a radial electric field, E ~ 200 kV/m, between the central electrode C (ℓ = 0.9 m, dia = 57 mm) and the annular electrode A. The current rises in 0.5 μs to a peak I_p = 180 kA and remains approximately constant for 3 μs. The radial current moves axially under the $\underline{J}_r \times \underline{B}_\theta$ force and rotates under the $\underline{J}_r \times \underline{B}_z$ force.

The magnetic field in the discharge was measured using multiple magnetic probes with 3 miniature coils (1.5 mm dia, good frequency response to 10 MHz) oriented to measure the three components of field (ie B_r, B_θ, B_z) simultaneously and independently. The coils were enclosed in a pyrex glass shield of 5 mm outside diameter. The axial electric field E_z was measured with two coaxial electric probes (1 mm tip dia). The first had an electrode separation of 10 mm which is comparable with the shock thickness and hence measures the average E_z field over a 10 mm extent of the shock structure. The second had an electrode separation of 100 mm which is somewhat larger than the shock thickness and hence can be used to measure the potential rise through the shock wave.

Further details of the apparatus and the measurement of initial plasma parameters may be found in CRAIG and PAUL (1973) and CRAIG (1974).

3. RESULTS

(a) General Flow Pattern

The shock and driving piston configuration of the low M_A results described in CRAIG (1974) is schematically shown in Fig. 1. A weakly curved shock front propagates ahead of a moving, diffuse, tilted current front which may be regarded as its driving piston. The shock is well separated from the driving piston at higher radii but merges with the piston towards the centre electrode. The propagation direction of the shock, ie the normal to the plane of the shock, is oblique to the initial field in the region of good separation. This general form of flow pattern was found to extend to lower initial field values. We describe detailed measurements of the shock structure for B_{z1} in the range 0 to 0.035 T, at a single position in the flow (r = 143 mm, z = 0.4 m) where the shock tilt was $\sim 30^{\circ}$ and the shock-piston separation good.

Oblique hydromagnetic shock waves have the properties that,

(i) the post-shock magnetic field is in the plane defined by the propagation direction and the pre-shock magnetic field.

(ii) the transverse magnetic field component increases across the shock,

(iii) the normal magnetic field is unchanged across the shock.

In our configuration we therefore have in the post-shock region, ie region 2 of Fig. 1,

$$B_{r2} > 0, \qquad B_{z2} > B_{z1} \qquad B_{\theta 2} = 0.$$

The magnetic field transition of the shock therefore requires a J_θ current. The piston involves current flow in the rz plane and may therefore be identified by a rise in B_θ.

Fig. 2(a) shows typical B_r and B_θ oscillograms as obtained with the multiple magnetic probe (B_{z1} = 0.011 T). We note the arrival of the shock (rise in B_r) occurs ~ 0.6 μs before the arrival of the piston (rise in B_θ). B_r drops in the piston region due to centrifugal effects associated with the $\underline{J}_r \times \underline{B}_z$ force. At lower B_{z1}, where the field transition of the shock is small, the shock can be more easily identified on an unintegrated $\dot{B}_r$ oscillogram (Fig. 2(b)).

A feature only present at low B_{z1} is a precursor rise in B_θ at the position of the shock (seen for example in Fig. 2(b) as the small precursor $\dot{B}_\theta$ peak ahead of the main piston peak). The probable explanation of this is that a small B_θ field diffuses ahead of the piston and is compressed in the shock. At higher B_{z1} values the shock and piston move faster (section 2(b)) and hence higher plasma conductivity will reduce such diffusion.

The tilt angle of the shock propagation to the initial field is given by (CRAIG, 1974),

$$\alpha = \mathrm{Tan}^{-1}\left(\frac{B_{z2} - B_{z1}}{B_{r2}}\right) = \mathrm{Tan}^{-1}\left(\frac{\dot{B}_z}{\dot{B}_r}\right).$$

This provides a convenient way of measuring the tilt angle of the shock. Fig. 2(c) illustrates such a measurement. From the peak $\dot{B}$ values we have $\alpha = 30^\circ$ for the case shown. The tilt angle was found to be essentially constant over the complete range of B_{z1}.

Fig. 2(d) shows a typical signal from the 10 mm electric probe together with $\dot{B}_r$ from an adjacent magnetic probe. Unlike $\dot{B}_r$ the electric probe signal at the shock is not sharply peaked. This

is due to the finite separation distance of the probe electrodes; an average E_z over 10 mm is measured. Fig. 2(e) shows a typical oscillogram from the 100 mm electric probe together with $\dot{B}_r$. The potential rise through the shock is seen in this case. Withdrawing the magnetic probe made no appreciable difference to the electric probe signals suggesting that perturbation effects are not serious. In Fig. 2(f) $\dot{B}_r$ and the 100 mm electric probe signal are expanded in time base in order to make detailed measurements of the shock structure. At lower B_{z1} values ($\lesssim$ 0.01 T) the electric probe signals show a region of negative potential ahead of the main rise (see Fig. 2(f)). This is taken to be evidence of a thermal wave at the front of the shock and is discussed in detail in a later section.

An unexplained feature on the $\dot{B}_r$ oscillograms, only occurring at $B_{z1} \gtrsim 0.007$ T, is illustrated in Fig. 2(g); a small precursor in $\dot{B}_r$ precedes the main $\dot{B}_r$ peak of the shock.

For very low B_{z1}, $\lesssim$ 0.002 T, the shock-piston separation decreases and some overlapping occurs. Fig. 2(h) shows $\dot{B}_r$ and $\dot{B}_\theta$ for the case B_{z1} = 0.001 T.

Fig. 2(i), (j) shows B_θ and the 10 mm electric probe signal for B_{z1}= 0.002 T and 0 T. The deformation of the baseline of the E_z traces ahead of the shock is due to electrical interference. The shock occurs at the foot of the piston. Again we note the region of negative potential ahead of the main potential rise of the shock. This is discussed in a later section.

(b) Axial Propagation

The axial velocities of the shock, V_{sz}, and the piston, V_{pz},

profiles were measured by axially scanning the magnetic probe. For a given B_{z1} value the propagation velocities decreased slowly with axial position. Fig. 3 shows the shock velocity at z = 0.4 m as a function of B_{z1}. We note a sharp decrease in velocity for fields below 0.01 T. For the lower field cases the arrival of the shock at z = 0.4 m occurs after the total applied radial current has reversed (ie after 4 μs). However it is found that when the applied current decreases the piston current does not drop but rather a reverse current front forms at z = 0 such that a propagating current loop is formed and there is no immediate effect on the piston. The 0.6 μs temporal shock separation of Fig. 2(a) for B_{z1} = 0.011 T therefore corresponds to 90 mm spatial separation. It should be noted that the true shock velocity is given by $V_s = V_{sz} \cos \alpha$.

The magnitude of B_r decreases only very slowly with axial position indicating a quasi-steady shock.

Also shown on Fig. 3 as functions of B_{z1} are the Alfven Mach number

$$M_A = \frac{V_s}{v_A} \quad \text{where } v_A = \frac{B_{z1}}{(\mu n_{e1} m_i)^{\frac{1}{2}}}$$

and the sonic Mach number

$$M_s = \frac{V_s}{a} \quad \text{where } a = \left(\frac{2\gamma k T_1}{m_i} \right)^{\frac{1}{2}} .$$

Pre-shock parameters $n_{e1} = 3 \times 10^{20}$ m^{-3} and $T_1 = 1.5 \times 10^4$ K are assumed. The critical Mach numer M_A^*, above which purely resistive shocks cannot exist, has been calculated by MURPHY (1971) for a general oblique hydromagnetic shock. All shocks discussed here are supercritical and should involve viscous dissipation.

(c) Comparison with Conservation Relation Theory.

The conservation relations may be solved to obtain the post-shock plasma parameters in terms of pre-shock parameters and the shock velocity. Fig. 4(a) shows both theoretical and experimental values of B_{r2} plotted as a function of B_{z1}. The theory assumes $n_{e1} = 3 \times 10^{20}$ m^{-3}, $T_{e1} = T_{i1} = 1.5 \times 10^{4}$ K, $\alpha = 30^{o}$ and V_{sz} varies with B_{z1} as shown in Fig. 3. The agreement is good over the range of B_{z1} considered.

Fig. 4(b) shows theoretical predictions of n_{e2} and $\frac{1}{2}(T_{e2} + T_{i2})$ plotted as a function of B_{z1}. In the following sections we use the notation n_{con} and $\frac{1}{2}T_{con}$ to denote these parameters. We have not, however, independently measured them.

(d) Shock Structure

Throughout the range of B_{z1} considered the magnetic field rise through the shock was found to be monotonic. At higher B_{z1} values the potential rise through the shock was monotonic but at lower fields ($B_{z1} \lesssim 0.01$ T) a region of negative potential preceded the main rise. We shall take the magnetic thickness L_{SB} and potential thickness L_{SV} of the shock to be the central 80% of the magnetic field rise (also corresponding to the distance between the 40% peak $\dot{B}$ positions) and the central 80% of the main potential rise respectively.

Fig. 5 shows experimental value of L_{SB} and L_{SV} plotted as a function of B_{z1}. The magnetic thickness L_{SB} is approximately constant at 25 mm for the complete B_{z1} range. The potential thickness L_{SV} is approximately constant, at 12 mm in the range 0.003 to 0.03 T. Measurement at very low B_{z1} becomes difficult because the potential rise of the shock merges into that of the piston. It

should be noted that the constancy of L_{SB} and L_{SV} is not instrumental because the magnetic field and potential rise times within the shock are not constant over the range of B_{z1} but the velocity variation happens to compensate.

(e) Electric Field Measurements

Fig. 6 shows the peak measured E_z from the short separation probe (ie the average over the central 10 mm of the shock) plotted as a function of B_{z1}. The dominant terms contributing to E_z are, from the generalised Ohms law,

$$E_z = -\frac{1}{en_e}\left(\frac{\partial p_e}{\partial z} + J_\theta B_r - J_r B_\theta\right).$$

The $J_r B_\theta / en_e$ term is negligible within the shock but is the dominant term in the piston region. The magnitude of J_θ within the shock, obtained directly from $\dot{B}_r$,

$$J_\theta \tilde{=} \frac{1}{\mu_o V_{sz}} \frac{\partial B_r}{\partial t}$$

is plotted in Fig. 6. Also shown in Fig. 6 are peak values of $J_\theta B_r / en_e$ based on the assumption that $n_e = 0.5\ (n_{con} + n_{e1})$ and $B_r = 0.5\ B_{r2}$ at the position of peak J_θ. This magnetic term therefore makes a negligible contribution to the measured E_z field for the lower B_{z1} values and the pressure gradient term therefore dominates.

4. DISCUSSION

(a) Comparison with Theoretical Structure

We compare our measurements with theoretical predictions of JUKES (1957-58). The variation of $2\lambda_{ii2}$ and B_{z1} is shown in Fig. 5 for the case $T_{i2} = \frac{1}{2}T_{con}$ and is in close agreement with the experimental L_{SV} for $B_{z1} \gtrsim 0.008$ T. Since $\lambda_{ii2} \propto T_{i2}^2$ it will however be sensitive to the ratio T_{i2}/T_{e2}. Our experimental result that, at low B_{z1}, L_{SV} exceeds the value of $2\lambda_{ii2}$ for $T_{i2} = \frac{1}{2}T_{con}$ suggests therefore that $T_{i2} > \frac{1}{2}T_{con}$, ie $T_{i2} > T_{e2}$, which is consistent with the

result of Jukes and also negligible Ohmic heating.

(b) Interpretation of Electric Probe Results

We take the region of negative potential at the front of the shock to be evidence of the precursor thermal wave predicted by Jukes. Until plasma flow impinges on the probe electrodes they will be surrounded by an electron rich sheath and have a potential lower than that of the surrounding plasma. In the initial plasma the probe tips are floating, ie no current is drawn, and the sheath potential has been calculated by CHEN (1965) to be

$$V = \frac{kT_e}{2e} \ln\left(\frac{\pi}{2}\frac{m}{N}\right) \simeq 4\ T_e(eV)\ \text{Volts}.$$

As the precursor thermal wave passes over the leading probe electrode the plasma potential increases by an amount $\delta V_p = k\delta T_e/e$ where δT_e is the increase in electron temperature in K out the sheath potential also increases by an amount $\delta V_s \simeq 3.5 \times 10^{-4}\ \delta T_e = 2.9\ \delta V_p$. The change in sheath potential therefore predominates and hence a negative probe signal is observed at the front of the shock structure. The positive probe signal that follows however indicates that the increasing plasma potential predominates over any sheath effects. This is due to two effects:

(i) The additional electric field term $\frac{kT_e}{en_e}\ \frac{dn_e}{dz}$ is present when the velocity transition reaches the probe electrode.

(ii) There is evidence that the fast flow in plasma shock waves causes a breakdown of the sheath around an electric probe electrode so that it then takes the plasma potential. For example, in the TARANTULA perpendicular shock wave experiment (PAUL et al, 1965) the change in directed ion energy in passing through the shock is entirely accounted for by the measured potential change across the shock which

is therefore assumed to be the change in plasma potential. If however the sheath was assumed to remain intact during the transit of the shock this would indicate a change in plasma potential sufficient to reflect the bulk of the ions which would then gyrate in the region ahead of the shock. Since the shock width was much less than the gyroradius this was not thought to happen and it was therefore concluded (PAUL 1975) that the sheath is somehow broken down by the plasma flow in the shock. Similarly, in the present experiment, if the sheath were assumed to remain in tact the change in sheath potential ($\sim 4(\frac{1}{2} T_{con} - T_{e1})$ assuming $T_{e2} \sim \frac{1}{2}T_{con}$ would exceed the change in plasma potential ($\sim L_{SV} E_{zAve}$). We conclude therefore that the plasma flow breaks down the sheath and the probe assumes plasma potential. In the case of the 100 mm electric probe where the electrode separation exceeds the overall shock thickness the absolute measurement of potential difference across the shock will be in error by the sheath potential of the preheat plasma which according to the above equation will be $\sim$ 5 volts. Our measurement of average electric field in the shock by the 10 mm probe should however be accurate because the flow will have destroyed the sheath at both electrodes.

It has been shown that the $\frac{1}{en_e} \frac{\partial p_e}{\partial z}$ term dominates the experimental E_z. We do not however derive any direct information on the individual variation of n_e and T_e through the shock. For simplicity we will assume their variations are well represented by the functions:

$$n_e = n_{e1} + \frac{(n_{con} - n_{e1})}{2}\left[1 + \text{erf}\left(\frac{1.917\ x}{L_{SN}}\right)\right]$$

$$T_e = T_{e1} + \frac{(T_{e2} - T_{e1})}{2}\left[1 + \text{erf}\left(\frac{1.917\ x}{L_{ST}}\right)\right]$$

where L_{SN} and L_{ST} are thickness of the central 80% of the density and temperature transitions respectively. Assuming various values of L_{SN}, L_{ST} and T_{e2}/T_{i2} we can then calculate values of L_{SV} and peak probe signal ($= \int_o^{10\,mm} E_z dz$) for comparison with experimental results in Figs. 5 and 6. In curve A $L_{SN} = L_{ST} = 10$ mm and $T_{e2} = T_{i2} = \frac{1}{2} T_{con}$; the probe signal is somewhat larger than experiment and L_{SV} slightly smaller than experiment. Curve B assumes a broader temperature structure ($L_{ST} = 20$ mm, $L_{SN} = 10$ mm, $T_{e2} = T_{i2} = \frac{1}{2} T_{con}$) which is more consistent with the precursor thermal wave; the probe signal becomes closer to the experimental values and L_{SV} is slightly larger than experiment. Curve C again assumes the broader thermal structure ($L_{ST} = 20$ mm, $L_{SN} = 10$ mm) but with incomplete equipartition with $T_{e2} = \frac{2}{3} T_{i2} = 2/5\ T_{con}$; the probe signal agrees closely with experiment and L_{SV} is only slightly modified at low B_{z1}.

(c) Dissipation Within the Shock

In the previous section we have discussed an electron shock structure ($L_{SN} = 10$ mm, $L_{ST} = 20$ mm, $T_{e2} = \frac{2}{3} T_{i2} = 2/5\ T_{con}$) which fits the experiment with regard to peak E_z and L_{SV}. We now consider whether classical ion heating in this structure is consistent with that required by the conservation relations.

The ion energy transfer equation in the shock frame of reference is

$$\frac{3}{2} nkv \frac{dT_i}{dx} = kvT_i \frac{dn}{dx} + \frac{4}{3} \mu \left(\frac{dv}{dx}\right)^2 - \frac{Kn^2}{T_e^{3/2}} (T_i - T_e)$$

where viscosity $\mu = 2.21 \times 10^{-16} \frac{T_i^{5/2}}{\ell n \Lambda}$ kgm m^{-1} s^{-1}

$$K = 8.14 \times 10^{-32} \ell n \Lambda \text{ J } m^3 \text{ } {}^{o}K^{\frac{1}{2}} \text{ } s^{-1}.$$

The terms on the right hand side of the equation represent adiabatic heating, viscous heating and equipartition. Using the above structure the ion heating falls below that required by the conservation relations by a factor of typically 3. However the viscous heating, which only occurs in the velocity transition, is the dominant ion heating mechanism and, because $\mu \propto T_i^{5/2}$, is critically dependent on the value of T_i at the foot of the velocity transition. This is in turn dependent on the exact structure of the precursor thermal wave and the degree of energy transfer to the ions occuring in it. For L_{SN} = 10 mm a T_i value of ~ 3.6 eV at the foot of the velocity transition is required to satisfy the conservation relations (T_{i2} = 3/2 T_{e2} = 3/5 T_{con}) over the complete range of B_{z1} considered. Such ion heating in the precursor thermal wave is reasonable in the cases of higher B_{z1} where the electron temperature in the thermal wave is significantly higher than 3.6 eV. However at lower B_{z1} ($\lesssim$ 0.005 T) where temperatures are lower such an amount of energy transfer will not occur and therefore a thinner velocity structure would be expected as is predicted by Jukes (Fig. 5).

The electron energy transfer equation in the shock frame of reference is

$$\frac{3}{2} nkv \frac{dT_e}{dx} = \eta J^2 + kvT_e \frac{dn}{dx} + \frac{d}{dx}\left(\lambda \frac{dT_e}{dx}\right) + \frac{Kn^2}{T_e^{3/2}}(T_i - T_e)$$

where η is the resistivity and λ is the thermal conductivity. We have ohmic heating, adiabatic heating, thermal conduction and equipartition terms. The ohmic heating is however negligible.

The main processes occurring in the shock are, therefore, (i) viscous heating of the ions in the main velocity transition, (ii) electron heating by equipartition with the ions towards the back of the shock, (iii) electron thermal conduction forward to produce the precursor thermal wave, (iv) ion heating by equipartition with the electrons in the thermal wave. Process (iv) in turn critically influences process (i).

(d) Effect of the Magnetic Field

Fig. 6 shows that the magnetic term contributing to E_z is small and as stated above classical ohmic dissipation is negligible. The main influence of the magnetic field is likely to be on the electron thermal conduction which will clearly be reduced by electron gyro motion in the transverse component of field. Such effects will be important for $\tau_{ee}\ \omega_{ce}\ \text{Sin}\ \theta \gtrsim 1$ which occurs for $B_{z1} \gtrsim 0.007$ T. Experimentally we find the precursor region of negative potential is not observed for $B_{z1} \gtrsim 0.01$ T. However if a precursor thermal wave is not present at higher B_{z1} the ion temperature at the foot of the velocity transition will be too small for the necessary viscous heating to occur in the observed structure; a thinner shock would be expected. BOGEN et al (1971) do, however, observe a precursor thermal wave even with an initial transverse field of ~ 0.013 T where $\tau_{ee}\omega_{ce} > 1$.

5. SUMMARY

We have produced a well separated oblique hydromagnetic shock over a range of small initial magnetic fields. At lowest field values the magnetic influence on the shock is negligible. The measured magnetic field transition across the shock is in good agreement with conservation relation theory for the measured velocity and initial plasma parameters. We therefore assume conservation theory values of post-shock density (n_e) and temperature ($T_e + T_i$) apply to the experiment.

The magnetic and potential structure of the shock have been measured. The potential structure is of primary importance because the magnetic influence on the shock dissipation is small. We have fitted a structure which uses conservation theory values of the density and temperature jump to the experimental values of the thickness and gradient of the potential structure of the shock. Our fitted structure is in general agreement with a full theoretical structure based on two fluid theory in that,

(i) there is evidence for the presence of a precursor thermal wave,

(ii) the thickness of the main potential rise is $\sim 2\lambda_{ii2}$,

(iii) the magnitude of the potential rise is consistent with $T_{e2} \sim T_{i2}$.

Exceptions to this agreement are

(a) At very low fields the potential structure is somewhat thicker than $2\lambda_{ii2}$. However separation from the driving piston is not complete at these fields.

(b) At higher fields $B_{z1} \gtrsim 0.01$ T there is no longer evidence of the precursor thermal wave and indeed the transverse component

of magnetic field would be expected to inhibit electron thermal conduction at these fields. If the thermal wave is not present and consequently no ion heating occurs ahead of the velocity transition then a structure somewhat thinner than $2\lambda_{ii2}$ would be required to produce the necessary viscous dissipation.

The author is grateful to Dr J.W.M. Paul and Dr P.T. Rumsby for many useful discussions and valuable suggestions, and to Dr R.J. Bickerton for his encouragement and support. Thanks are due to Mr L.S. Holmes for technical assistance.

REFERENCES

BOGEN P., DIPPEL K.H., HINTZ E. and SIEMSEN F. (1971) Proc. 10th Conf on Phenomona in Ionized Gases, Oxford.

CHEN F.F. (1965) Ch. 4 of 'Plasma Diagnostic Techniques' Ed. Huddlestone R.H. and Leonard S.L., Academic.

COHN D.B. and MACKENZIE K.R. (1972) Phys. Rev. Lett. 28, 656.

CRAIG, A.D. (1974) J. Plasma Phys. 12, 129.

CRAIG A.D. and PAUL J.W.M. (1973) J. Plasma Phys. 9, 161.

HONZAWA T. (1973) Plasma Physics 15, 467.

JUKES J. D. (1957-58) J. Fluid Mech. 3, 275.

MURPHY R.V.W. (1971) D Phil Thesis, University of Oxford.

PAUL J.W.M., HOLMES L.S., PARKINSON M.J. and SHEFFIELD J. (1965) Nature 208, 134.

PAUL J.W.M. (1970) Physics of Hot Plasmas (ed. B.J. Rye and J.C. Taylor), p.302, Oliver and Boyd.

PAUL J.W.M. (1975) Private communication.

TAYLOR R.J., BAKER D.R. and IKEZI H. (1970) Phys. Rev. Lett. 24, 206.

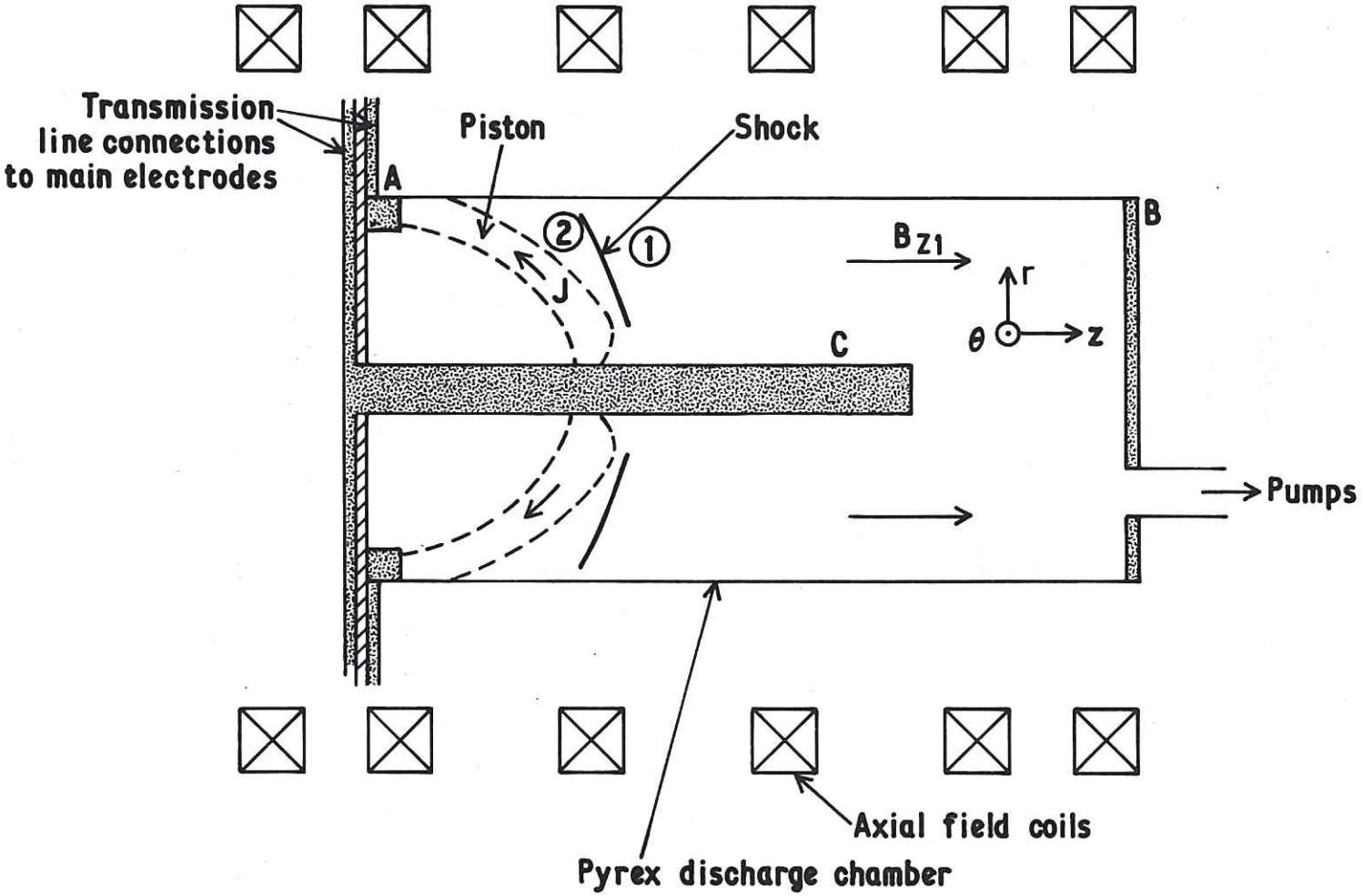

Fig.1 Schematic of apparatus and basic plasma flow pattern.

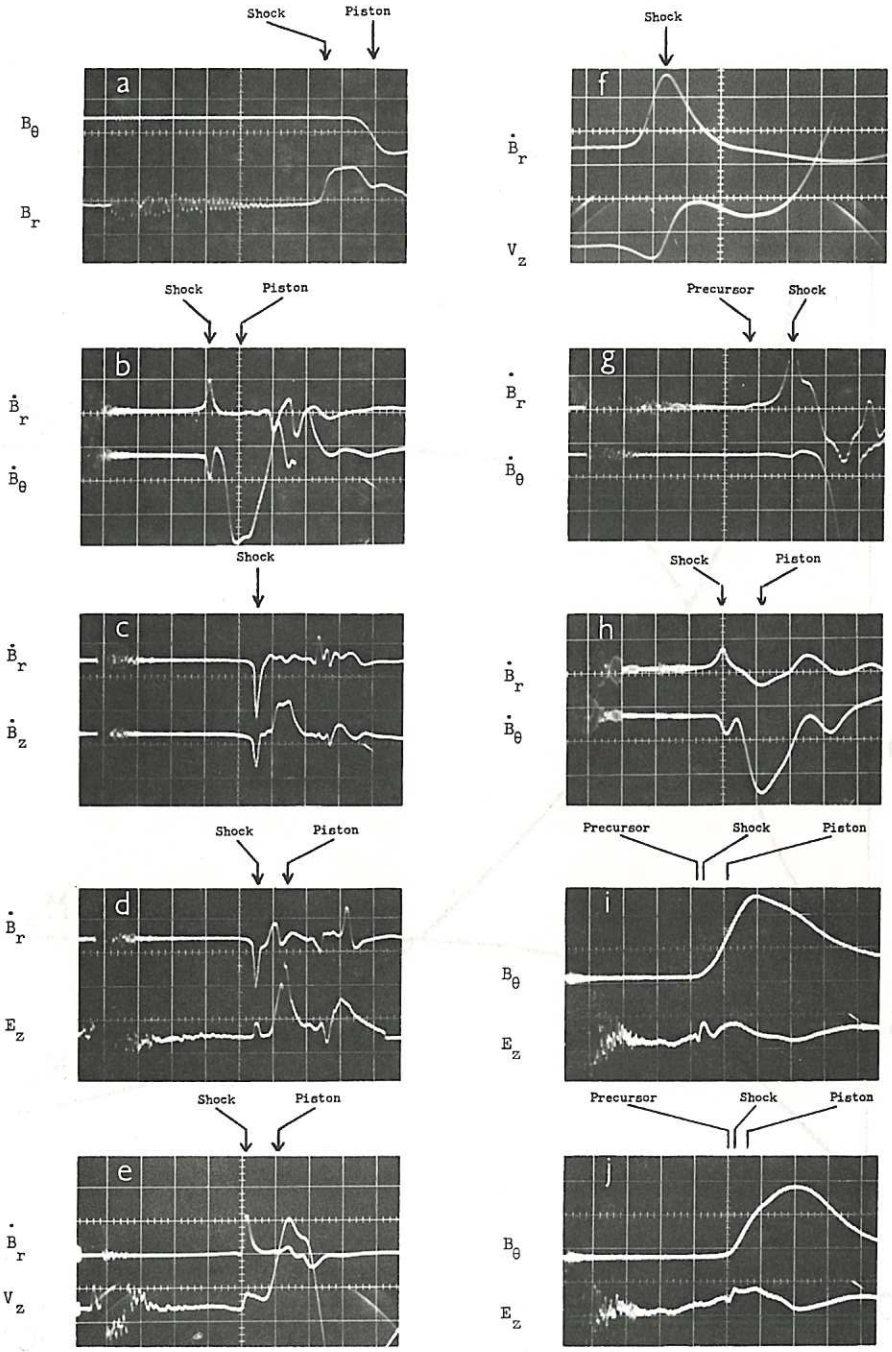

Fig.2 Typical oscillograms:

(a) B_{Z1} = 0.011 T, B_θ (0.14 T/div, 0.5 μs/div), B_r (0.014 T/div, 0.5 μs/div).

(b) B_{Z1} = 0.004 T, $\dot{B}_r$ (2.65 x 10^4 Ts^{-1} /div, 1 μs/div), $\dot{B}_\theta$ (2.65 x 10^4 $T\,s^{-1}$ /div, 1 μs/div).

(c) B_{Z1} = 0.011 T, $\dot{B}_r$ and $\dot{B}_Z$ (5.3 x 10^4 $T\,s^{-1}$ /div, 1 μs/div).

(d) B_{Z1} = 0.011 T, $\dot{B}_r$ (5.3 x 10^4 $T\,s^{-1}$ /div, 1 μs/div), E_Z (2 x 10^3 $V\,m^{-1}$ /div, 1 μs/div).

(e) B_{Z1} = 0.0074 T, $\dot{B}_r$ (2.65 x 10^4 $T\,s^{-1}$ /div, 1 μs/div), V_Z (20 V/div, 1 μs/div).

(f) B_{Z1} = 0.011 T, $\dot{B}_r$ (1.3 x 10^4 $T\,s^{-1}$ /div, 0.2 μs/div), V_Z (10 V/div, 0.2 μs/div).

(g) B_{Z1} = 0.011 T, $\dot{B}_r$ (2.65 x 10^4 $T\,s^{-1}$ /div, 0.5 μs/div), $\dot{B}_\theta$ (1.32 x 10^5 $T\,s^{-1}$ /div, 0.5 μs/div).

(h) B_{Z1} = 0.001 T, $\dot{B}_r$ (5.4 x 10^3 $T\,s^{-1}$ /div, 1 μs/div), $\dot{B}_\theta$ (1.32 x 10^4 $T\,s^{-1}$ /div, 1 μs/div).

(i) B_{Z1} = 0.002 T, B_θ (0.014 T/div, 2 μs/div), E_Z (5 x 10^2 $V\,m^{-1}$ /div, 2 μs/div).

(j) B_{Z1} = 0 T, B_θ (0.014 T/div, 2 μs/div), E_Z (5 x 10^2 $V\,m^{-1}$ /div, 2 μs/div).

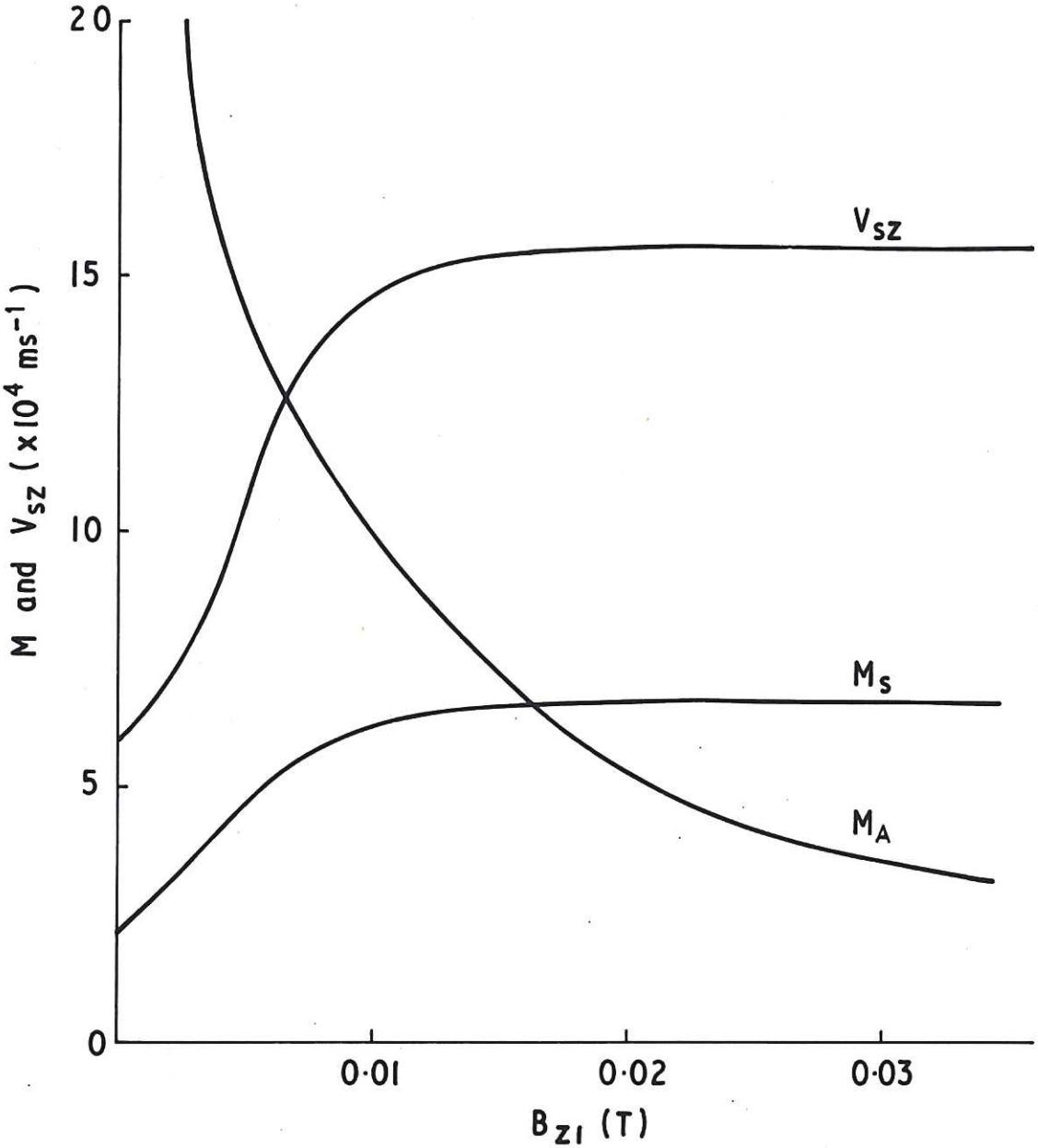

Fig.3 Axial velocity of shock V_{SZ}, Alfven Mach number M_A and sonic Mach number M_S plotted against initial magnetic field B_{Z1}.

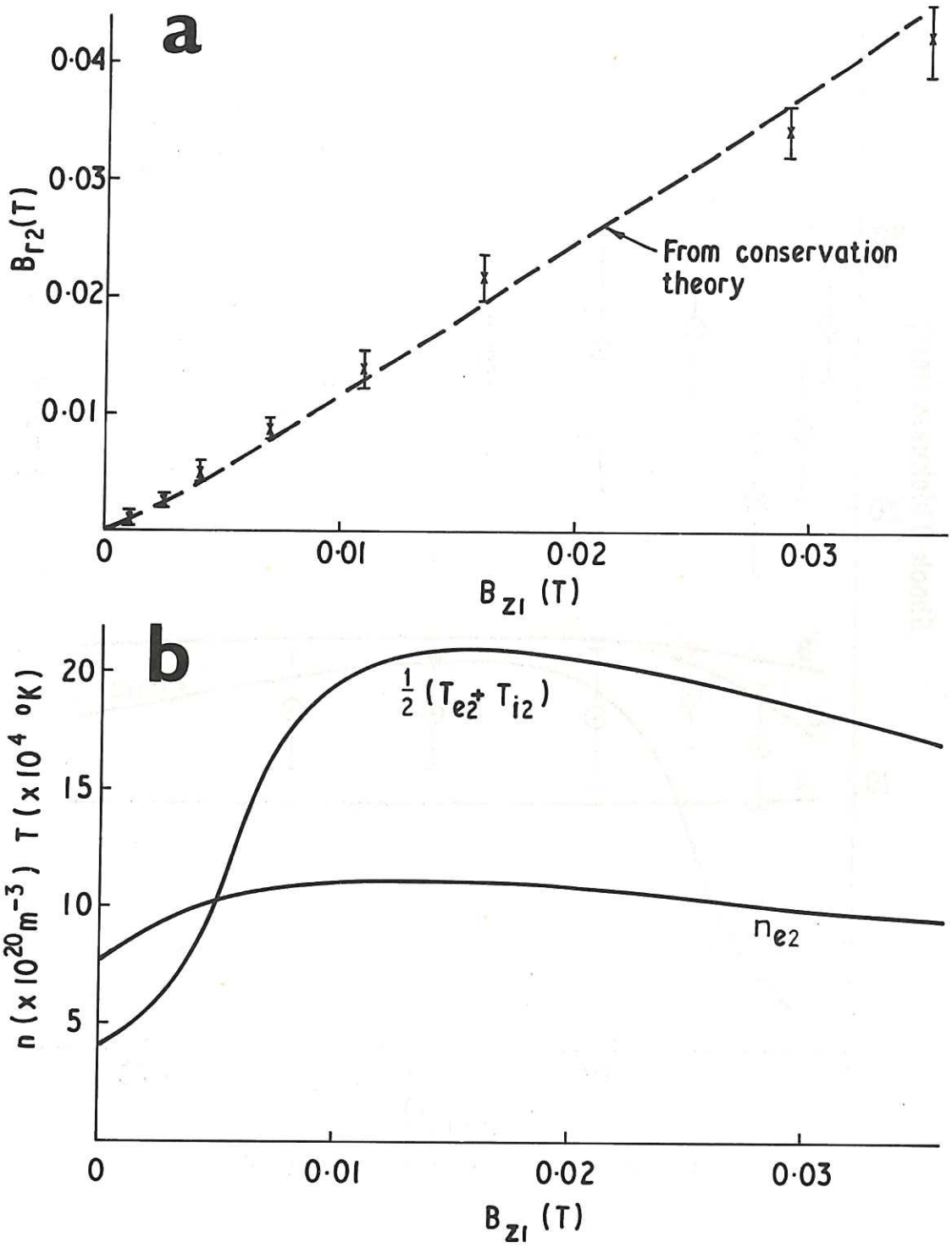

Fig.4 (a) Experimental and theoretical variation of B_{r2} with B_{z1}.
(b) Theoretical prediction of n_{e2} and ½ (T_{e2} + T_{i2}) versus B_{z1}.

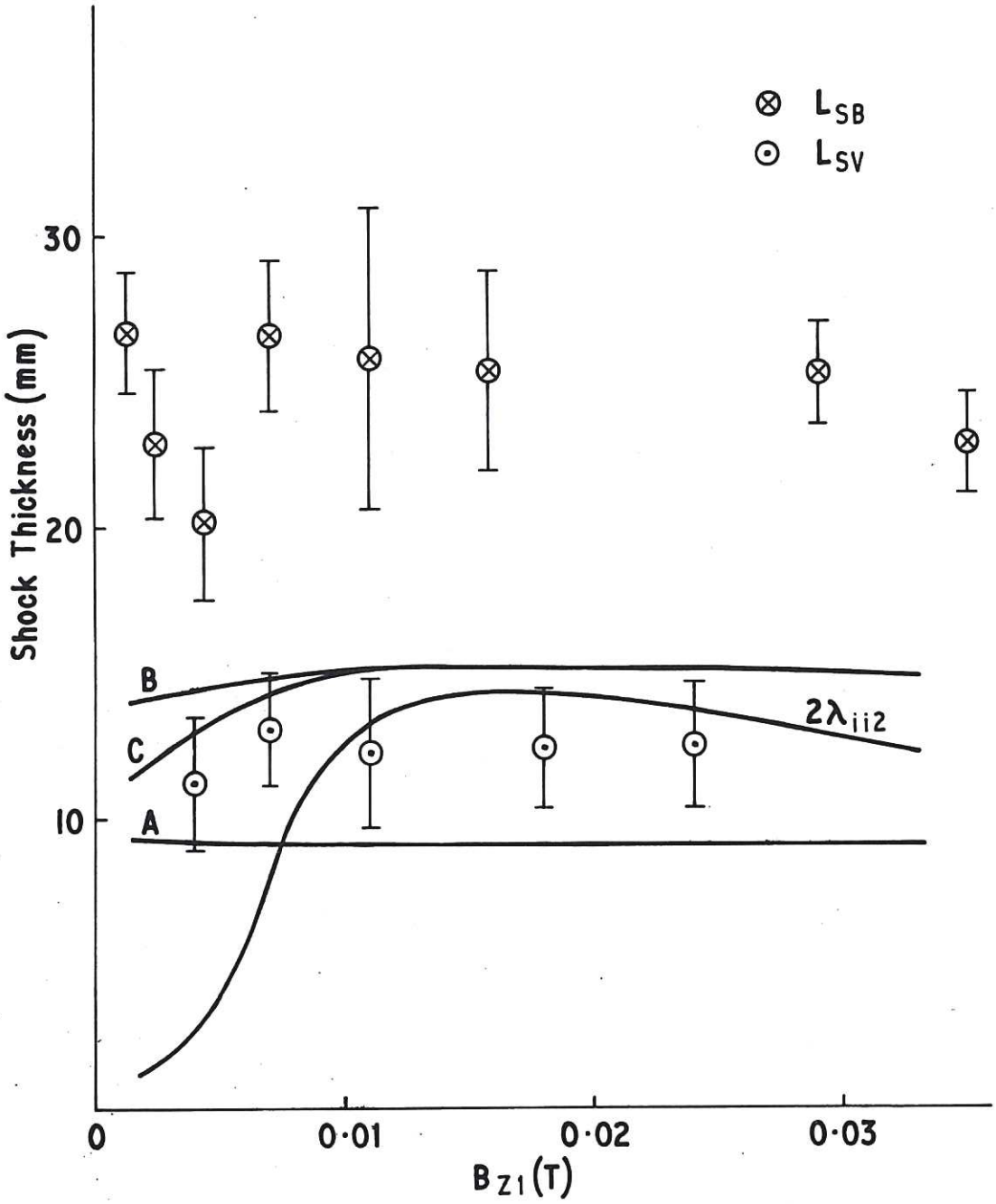

Fig.5 Shock thickness versus initial magnetic field B_{Z1}.

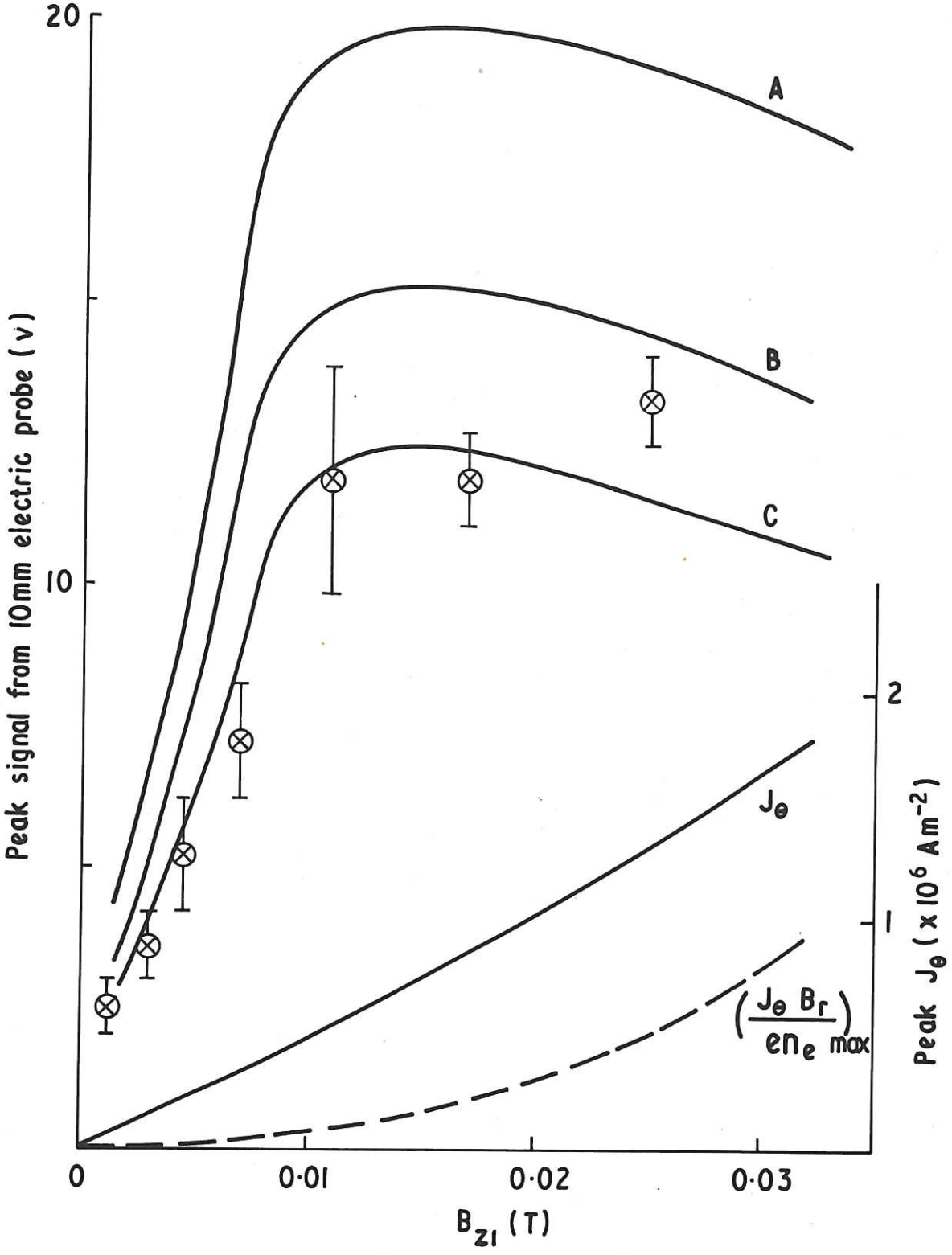

Fig.6 Variation of peak E probe signal and peak J_θ with B_{z1}.